Characterization of the $BaBiO_3$-doped $BaTiO_3$ positive temperature coefficient of a resistivity ceramic using impedance spectroscopy with $T_c = 155$ °C*

Yuan Chang-Lai(袁昌来)[a)b)†], Liu Xin-Yu(刘心宇)[a)b)], Zhou Chang-Rong(周昌荣)[b)], Xu Ji-Wen(许积文)[b)], and Yang Yun(杨 云)[b)]

[a)] *College of Materials Science and Engineering, Central South University, Changsha* 410083, *China*

[b)] *School of Material Science and Engineering, Guilin University of Electronic Technology, Guilin* 541004, *China*

(Received 16 June 2010; revised manuscript received 8 December 2010)

$BaBiO_3$-doped $BaTiO_3$ (BB–BT) ceramic, as a candidate for lead-free positive temperature coefficient of resistivity (PTCR) materials with a higher Curie temperature, has been synthesized in air by a conventional sintering technique. The temperature dependence of resistivity shows that the phase transition of the PTC thermistor ceramic occurs at the Curie temperature, $T_c = 155$ °C, which is higher than that of $BaTiO_3$ (≤ 130 °C). Analysis of ac impedance data using complex impedance spectroscopy gives the alternate current (AC) resistance of the PTCR ceramic. By additional use of the complex electric modulus formalism to analyse the same data, the inhomogeneous nature of the ceramic may be unveiled. The impedance spectra reveal that the grain resistance of the BB–BT sample is slightly influenced by the increase of temperature, indicating that the increase in overall resistivity is entirely due to a grain-boundary effect. Based on the dependence of the extent to which the peaks of the imaginary part of electric modulus and impedance are matched on frequency, the conduction mechanism is also discussed for a BB–BT ceramic system.

Keywords: $BaBiO_3$-doped $BaTiO_3$, positive temperature coefficient thermistor, impedance spectroscopy, high T_c

PACS: 87.19.rf, 84.32.Ff, 81.05.Je, 82.56.Na **DOI:** 10.1088/1674-1056/20/4/048701

1. Introduction

$BaTiO_3$-based ceramic materials are widely believed to have a positive temperature coefficient of resistivity (PTCR), and it is regarded as a ferroelectric and piezoelectric material. It is well known that insulating $BaTiO_3$ (BT) ceramics can easily achieve n-type semiconductivity with the addition of a small quantity of donor dopants such as La^{3+}, Nb^{5+}, Ta^{5+}, etc.[1−3] Acceptors such as Mn increase the height of the grain boundary barrier by activating deep trap states.[4] Doped semiconducting $BaTiO_3$ ceramics can often show a sudden increase in resistivity above the Curie point, T_c (i.e., PTCR phenomenon). The PTCR characteristic is closely associated with the ferroelectric Curie point, T_c. Isovalent substitutions of Pb^{2+} ($PbTiO_3$, $T_c = 490$ °C) for Ba^{2+} of BT is necessary if the PTCR material is to have a higher Curie temperature than the T_c of BT ($T_c = 120$ °C ~ 130 °C).[5] Currently, it is believed that no one can fabricate PTCR materials with $T_c > 130$ °C without the addition of $PbTiO_3$.

During the last few years, increased awareness of environmental topics has spurred considerable efforts to reduce the quantity of hazardous substances in consumer products. Despite all these efforts, so far there has been no suitable marketized material to replace PTCR ceramics containing toxic lead, such as the ubiquitous (Ba, Pb)TiO_3 in temperature sensor applications. Recent research work has focused mainly on a lead-free $Bi_{0.5}Na_{0.5}TiO_3$–$BaTiO_3$ (BNT–BT) system with a perovskite-type structure.[6−9] To some extent, a BNT–BT system is a promising lead-free PTCR material with $T_c > 130$ °C.

However, to obtain the PTCR characteristic, the BNT–BT ceramic system needs to be sintered in the N_2 flow of a low O_2 concentration.[10] In particular, the sintering conditions, especially the concentration of O_2 in the N_2 flow, must be well controlled. For large-scale industrial production, it is very difficult to fabricate high T_c lead-free PTCR materials in such extreme preparation conditions.

*Project supported by the Research Funds of the Guangxi Key Laboratory of Information Materials at the School of Material Science and Engineering, China (Grant No. 0710908-07-Z).

†Corresponding author. E-mail: yclguet@yahoo.com

© 2011 Chinese Physical Society and IOP Publishing Ltd

In the present study, a lead free $BaBiO_3$-doped $BaTiO_3$ (BB–BT) PTCR thermistor with low resistivity and T_c = 155 °C is directly prepared in air. Complex impedance spectroscopy (CIS) is a powerful tool to analyse the dielectric and electrical characterizations of thermistor ceramics,[11,12] and thus it is also used to investigate the electrical properties of BB–BT ceramic. More information about electrical properties, obtained by the CIS, is expected to explain the PTCR phenomena comprehensively in the semiconducting BB–BT ceramic system.

2. Experimental details

$BaTiO_3$ powder was prepared in air by a conventional solid state technique using appropriate stoichiometric mixtures of high-purity (99.99%) $BaCO_3$ and TiO_2 powders. $BaBiO_3$ powder was also prepared by a similar technology. A mixture of three materials with a molar ratio of $BaTiO_3$:$BaBiO_3$:SiC (the sintering additive) of 100:0.5:0.5 was ball milled for 12 h, dried, and uniaxially pressed into disks of 16 mm in diameter and 1.6 mm in thickness under 200 MPa with using polyvinyl alcohol (PVA) as a binder. After burning off the PVA, the disks directly placed on a high-alumina sheet were sintered in air at 1280 °C for 60 min, in a tube furnace. The obtained samples were polished. For the electrical and the CIS measurements, the Al paste was pasted on both sides of the samples as the electrodes and then heated at 600 °C for 40 min.

The resistivity was determined using a digital resistance meter (Fluker 45) from 25 °C to 300 °C at a heating ratio of 5 °C/min. Impedance spectroscopy was performed using an Agilent (4294A) impedance analyser with computer controlled automated data collection. The measurements were carried out in a frequency range from 5 Hz up to 1 MHz and in the temperature range from 25 °C to 280 °C.

3. Results and discussion

The x-ray diffraction (XRD) pattern of the sintered ceramic of BB–BT is shown in Fig. 1. The phase of BT can be identified from the XRD pattern of the sintered BT–BNT ceramic. However, the BB phase cannot be identified due to the lack of diffraction peaks. The BB–BT ceramic at room temperature exhibits a tetragonal structure similar to that of the pure BT sample. The inset in Fig. 1 shows the scanning electron microscopy (SEM) micrograph of the as-sintered BB–BT. The average grain diameter is about 40 μm, which is obviously larger that that of ordinary $BaTiO_3$-based PTC ceramics. Generally, the samples with abnormal grain growth are relatively stable to the global reoxidation, and their grain boundary properties can be changed by the temperature-induced reoxidation process.

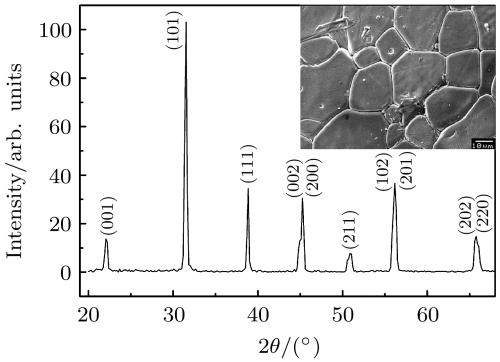


Fig. 1. The XRD pattern of the sintered ceramic of BB–BT. The inset shows the SEM image of BB–BT ceramic.

The temperature dependence of direct current (DC) resistivity of the BB–BT sample with 0.5 mol% $BaBiO_3$ is plotted in Fig. 2. The electrical resistivity of BB–BT at temperatures below 140 °C behaves like that of any semiconductor with a negative temperature coefficient. A sudden increase in resistivity starting at 155 °C and ending at 280 °C is observed. In this region the resistivity increases exponentially with temperature. This abrupt increase in resistivity is attributed to the shift from tetragonal phase (ferroelectric) to cubic phase (paraelectric), which is evidence of the PTC (positive temperature coefficient) effect. The PTC magnitude, defined as $\log(\rho_{max}/\rho_{min})$, where ρ_{max} is the peak resistance and ρ_{min} is the minimum measured value, normally occurring just below T_c, is about 2 in the disk that was sintered in air at 1280 °C.

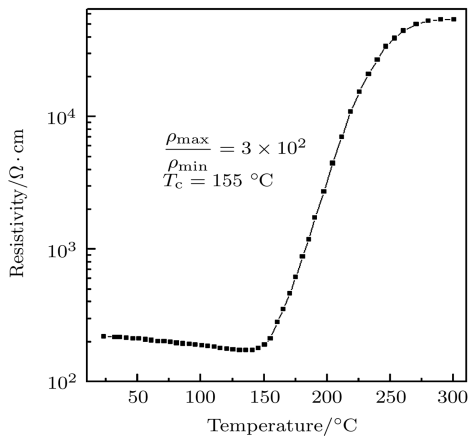


Fig. 2. Temperature dependence of resistivity for sample BB–BT sintered at 1280 °C.

The most widely accepted model of the PTCR effect[13−15] is based on the existence of Schottky potential barriers caused by electron acceptor states at grain boundaries. Later, the PTC effect has been further explained in terms of double-Schottky-barrier model.[16,17] The majority of charge carriers (electrons in the case of donor-doped $BaTiO_3$) are trapped by acceptor states in the grain boundary core region, which gives rise to a negative net-charge of the grain boundary core and adjacent space charge layers in the grains where the majority of charge carriers are depleted. At temperatures below T_c, the potential barrier height and, consequently, the contribution of the space charge layer to the grain boundary resistance are expected to vanish because of the compensation of the interfacial charges by the spontaneous ferroelectric polarization. Above T_c, due to the disappearance of spontaneous polarization, the resistivity of the PTCR material is controlled by the height of the potential barrier.

To reveal the origin of the PTCR effect in the BB–BT sample, AC complex impedance spectroscopy is also performed for analysing the resistivity properties of BB–BT sample in a temperature range of 25 °C–280 °C. The impedance data $[Z^*(\omega)]$ are commonly plotted in the complex plane, a plot of real component $[\mathrm{Re}Z(\omega)]$ versus imaginary component $[\mathrm{Im}Z(\omega)]$. $Z^*(\omega)$ is represented by

$$\begin{aligned} z^*(\omega) &= \mathrm{Re}Z(\omega) + \mathrm{j}\,\mathrm{Im}Z(\omega) \\ &= Z_{\mathrm{g}}^*(\omega) + Z_{\mathrm{gb}}^*(\omega), \end{aligned} \tag{1}$$

where g stands for grain and gb for grain boundary.

For the PTC thermistor ceramic, typical complex plane representations of impedance data are depicted in Fig. 3. Below the Curie temperature, $T_c = 155$ °C,

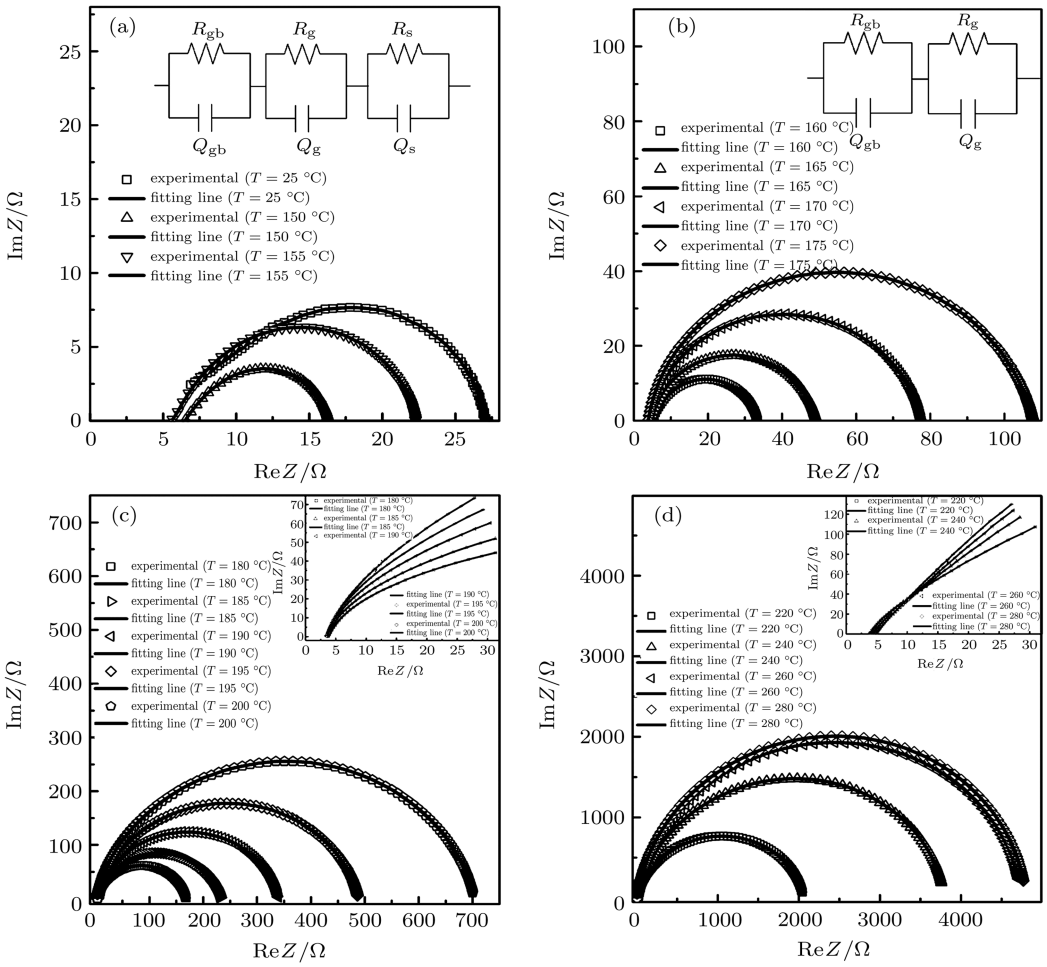


Fig. 3. Comparisons between the measured impedance spectroscopic results with the fitting results for the BB–BT ceramic at (a) T = 25 °C–155 °C, (b) T = 160 °C–175 °C, (c) T = 180 °C–200 °C, and (d) T = 220 °C–280 °C. Inset in Fig. 3(a) shows the equivalent circuit model at T = 25 °C–155 °C; inset of Fig. 3(b) exhibits the equivalent circuit model at $T \geq 160$ °C; insets in Figs. 3(c) and 3(d) display the magnified impedance spectra in a high frequency region.

the impedance spectra are characterized by one depressed and asymmetric distorted semicircle with a nonzero high frequency intercept at the real axis (Fig. 3(a)). At temperatures above T_c, only one depressed semicircle is observed (Figs. 3(b)–3(c)). The behaviour of the electrical response obeys the Cole–Cole's formalism.[18] The depression of the semicircles is considered further as evidence of a polarization phenomenon with a distribution of relaxation times. The insets in Figs. 3(c) and 3(d) show the high frequency intercept in the magnified impedance complex plane plot. The contribution positioned at low frequencies, corresponds to the grain boundary response. In the higher-frequency range, the contribution corresponds to a specific property of the grain. In a high- or mid-frequency range, the contribution corresponds to resistive grain shell in outer grain region.[19] In Fig. 3(a), the shape of diagram indicates that the electrical response is composed of at least two semicircles corresponding to grain boundary and grain shell, both contributions exhibiting an overlapping and decentralization degree. For Figs. 3(b)–3(d), the symmetric depressed semicircle is attributed to the contribution of grain boundary. At the same time, it is observed from Fig. 3(a) to Fig. 3(d) that there is a nonzero high frequency intercept at the real axis. The intercept is correlated to the grain contribution.[8] Thus, in Fig. 3(a), the electric properties of BB–BT sample can be represented by three parallel RC-equivalent circuits in series and the electrical responses of Figs. 3(b)–3(d) by two parallel RC-equivalent circuits in series. Hence, below T_c (Fig. 3(a)), the electrical response of the PTC ceramic is mainly composed of three components of grain boundary (R_{gb}), grain (R_g) and grain shell (R_s). Above T_c (Figs. 3(b)–(d)), the scenario can be that the contributions of electrical response are attributed mainly to the grain boundary (R_{gb}) and the grain (R_g).

It is well known that each parallel RC element like grain boundary gives rise to a semicircle in the complex plane plots of impedance (Re$Z(\omega)$ versus Im$Z(\omega)$), and the electrical modulus (Re$M(\omega)$ versus Im$M(\omega)$). The electric modulus can be derived by the following equation:

$$M^*(\omega) = \mathrm{j}\ \omega C_0 z^*(\omega) = \mathrm{Re}M(\omega) + \mathrm{j}\ \mathrm{Im}M(\omega), \quad (2)$$

where C_0 is the vacuum capacitance of the cell.

Spectroscopic plots of Im$Z(\omega)$ and Im$M(\omega)$ versus log f give a Debye peak for each RC element in the Im$Z(\omega)$ and the Im$M(\omega)$ spectra which are described by

$$\mathrm{Im}Z(\omega) = R\left[\frac{\omega RC}{1+(\omega RC)^2}\right], \quad (3)$$

and

$$\mathrm{Im}M(\omega) = \frac{\varepsilon_0}{C}\left[\frac{\omega RC}{1+(\omega RC)^2}\right], \quad (4)$$

where $\omega = 2\pi f$ is the angular frequency (f is the applied frequency in hertz) and ε_0 is the permittivity of free space, 8.854×10^{-14} F/cm.

The frequency and magnitudes of Im$Z(\omega)$ and Im$M(\omega)$ at the Debye peak maxima for each RC element are given as

$$\omega_{max} = 2\pi f_{max} = 1/RC, \quad (5)$$

$$\mathrm{Im}Z_{max} = R/2, \quad (6)$$

and

$$\mathrm{Im}M_{max} = \varepsilon_0/2C. \quad (7)$$

Hence, the magnitudes of R and C for each electrical component can be determined from the intercepts in the complex plane plots or estimated from either Im$Z(\omega)$ or Im$M(\omega)$, using Eqs. (5)–(7). Moreover, taking into account the depressed semicircles in Figs. 3(a)–3(d), the ideal character of the electrical components is represented by the Q parameter instead of ideal capacitance (C). In this way, Q represents a nonideal capacitance that is, in physics, determined by parameters Y_0 and exponent n with $n \leq 1$. The C is derived from the following equation:

$$C = R^{[(1-n)/n]}Y_0^{(1/n)}, \quad (8)$$

Y_0 tends to C, when the exponent n tends to a value of 1. The departure from ideal character exhibited by parameter Q is due exclusively to the distribution of relaxation times, which leads to the decentralization phenomenon of the semicircle. According to the above analyses of electrical response and nonideal character, corresponding equivalent circuits obtained above T_c and below T_c are shown in the insets of Figs. 3(a) and 3(b) respectively. The empirical circuits shown in the inset of Figs. 3(a) and (b) are used for the evaluation of all impedance spectra by complex nonlinear least squares fitting method. The fitting curves are also shown in Fig. 3 from 25 °C to 280 °C. The points on the impedance diagrams are the experimental data, while the solid line represents the theoretical fitting. The experimental data are in good agreement with the fitting curves.

Figure 4 shows the temperature dependences of the resistance values of R_s (by curve) and the R_g and R_{gb} (by the inset table). It can be seen that the variation of resistance of the BB–BT sample is determined mainly by that of the resistance from the grain boundary component. The grain resistance (see the inset table in Fig. 4) remains almost constant throughout the whole temperature range. Below T_c, the magnitude of grain shell resistance is almost equal to that of grain resistance. Above T_c, the contribution of grain shell resistance disappears due to the lower value of resistance. However, a rapid rise starting from T_c and the PTCR effect are observed in R_{gb} of the BB–BT sample, which shows that the transition temperature of grain boundary resistance keeps the same pace as that of ceramic resistance. It is concluded that only the grain boundary can contribute to the PTCR effect of the BB–BT ceramic. Based on the forgoing analysis, it can be speculated that the abrupt of the grain boundary resistance can originate from the reoxidation of grain boundary.

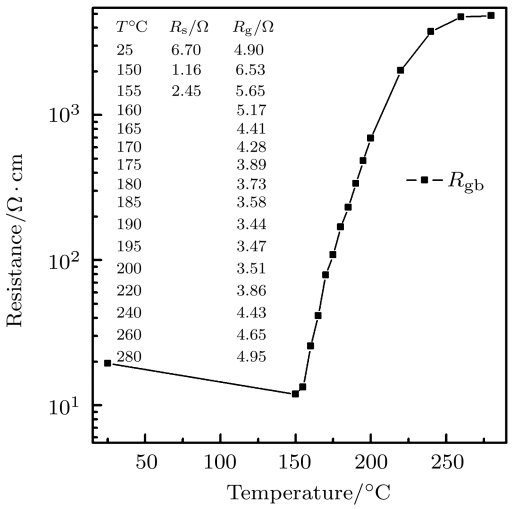


Fig. 4. Grain boundary resistance (R_{gb}) as a function of temperature. The inset table shows the magnitudes of grain resistance and grain shell resistance at different temperatures.

Figures 5(a) and 5(b) show imaginary parts Im$Z(\omega)$ and Im$M(\omega)$ of the electric modulus each as a function of logarithmic frequency for BB–BT sample at several temperatures, respectively. Only a part of the curves of Im$Z(\omega)$ and Im$M(\omega)$ are obtained due to the uncovered high frequencies at 25 °C. In the temperature range 150 °C $\leq T \leq$165 °C, a single, almost Debye-like peak is observed in each Im$Z(\omega)$ spectrum. However, in the same temperature range, the peak of Im$M(\omega)$ curve is still not observed. Above T = 165 °C, the peak of Im$M(\omega)$ curve occurs in each Im$Z(\omega)$ spectrum, and their peak frequencies, i.e. f_{Mp} and f_{Zp}, are in complete discordance with each other. The presence of an appreciable mismatch between Im$M(\omega)$ and Im$Z(\omega)$ peaks for the whole temperature range is important evidence of localized conduction.[20,21] The overlapping of peaks of Im$M(\omega)$ and Im$Z(\omega)$ curves is key evidence of delocalized conduction.[20] From Figs. 5(a) and 5(b) it can be seen that with temperature increasing, the peaks of Im$M(\omega)$ and Im$Z(\omega)$ curves tend to overlap, indicating the conduction process from short-range conductivity to probable long-range conductivity. Below T = 195 °C, an obvious asymmetric character of peak of each Im$Z(\omega)$ curve at frequencies above maximum frequency (f_{max}) is observed, which suggests the contribution of the lattice defect or structural aspects to the conduction relaxation.[22] With temperature increasing, the asymmetric phenomenon is gradually weakened. Above T = 195 °C, the peak of each Im$Z(\omega)$ curve at frequencies above f_{max} tends to be of excellent symmetry with temperature rising. Hence, these mean that the contribution of the lattice defect or structural aspects to the conduction relaxation reduces with temperature increasing, and almost disappears after the measured temperature T = 195 °C.

Although the peak values mismatch with each other between f_{Zp} and f_{Mp} in Fig. 5, both the f_{Zp} and f_{Mp} occur at low frequencies ($< 10^6$ Hz), indicating the two peaks result from the same RQ element. Because of the maximal value of Im$Z(\omega)$ curve and its location at the lower frequency, it is reasonable to attribute this RQ element to the component of the grain boundary. For the reason why the grain positioned in the higher frequency range shows no peaks of Im$M(\omega)$ and Im$Z(\omega)$, the peaks of Im$M(\omega)$ and Im$Z(\omega)$ associated with grains are considered to be outside the measured frequency range ($> 10^7$ Hz). Furthermore, it is well known that the Im$M(\omega)$ curve tends to zero at low frequencies, suggesting that the electrode polarization phenomenon is negligible or absent.

The frequency region below f_{Mp} determines the range in which charge carriers are mobile over long distances. In the frequency range above f_{Mp}, the carriers are confined in potential well, being movable over a short distance. The peak of ImM curve in relation to the Im$Z(\omega)$ peak shifts toward lower frequencies over a temperature range of 25 °C–260 °C but then slightly shifts back to higher frequency with temperature increasing up to 280 °C. The shift of peak fre-

quency plays an important role in the magnitudes of the relaxation time of grain boundary resistance and grain boundary capacitance (i.e., $\tau_{Z\mathrm{gb}}$ and $\tau_{M\mathrm{gb}}$, respectively). According to Eq. (5), the decrease of $f_{Z\mathrm{p}}$ and $f_{M\mathrm{p}}$ values denotes the increase of $\tau_{Z\mathrm{gb}}$ and $\tau_{M\mathrm{gb}}$ with temperature rising.

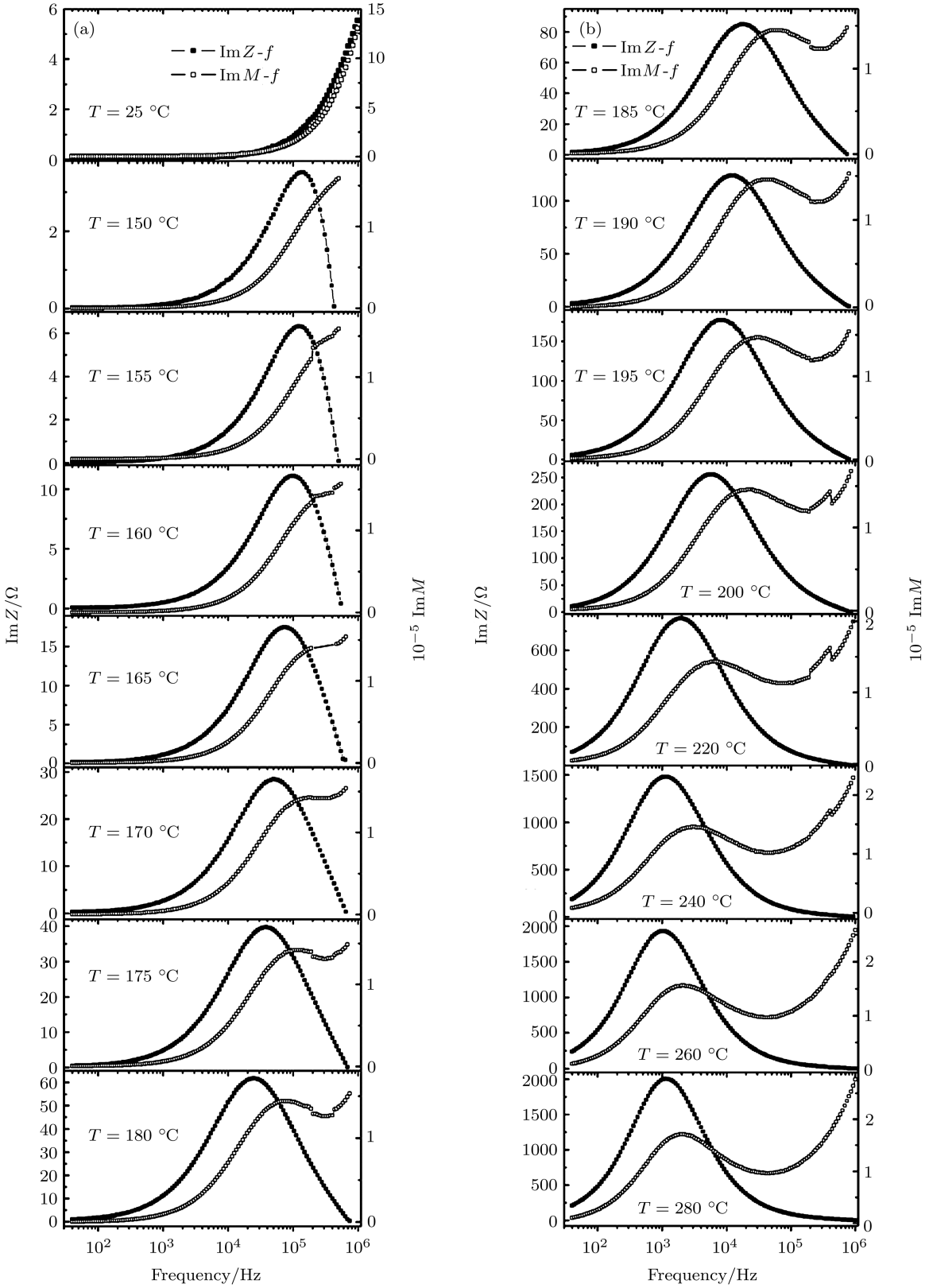


Fig. 5. Impedance ImZ and modulus ImM spectroscopic plots at different temperatures for BB–BT ceramic.

According to the character of Fig. 5, below 280 °C, the two peaks that describe the same relaxation process (grain boundary relaxation behaviour) completely disaccord with the following order proposed elsewhere: $\tau_{Z\mathrm{gb}} > \tau_{M\mathrm{gb}}$.

For the thermistor ceramic based on $BaTiO_3$, the $BaBiO_3$ dopant is a key impact factor for the semiconduction and the phase temperature with $T_c = 155$ °C. It is reported that, the crystal structure of $BaBiO_3$ is a distorted perovskite with two kinds of Bi sites, namely "Bi^{3+}" and "Bi^{5+}".[23] For achieving the semiconducted $BaTiO_3$, a small number of Bi^{3+} ions will substitute for Ba^{2+} in the lattices and Ti^{4+} ions will partly be replaced by Bi^{5+} after the $BaBiO_3$ has been added.[24] The reaction occurs as shown below:[25]

$$\begin{aligned} & x\mathrm{Ba_2Bi^{3+}Bi^{5+}O_6} + 2\mathrm{BaTiO_3} \\ = {} & (\mathrm{Ba^{2+}_{1-x}Bi^{3+}_x})[\mathrm{Ti^{4+}_{1-x}}(\mathrm{Ti^{4+}}\cdot \mathrm{e})_x]\mathrm{O_3} \\ & + \mathrm{Ba^{2+}}[\mathrm{Ti^{4+}_{1-2x}Bi^{5+}_x}(\mathrm{Ti^{4+}}\cdot \mathrm{e})_x]\mathrm{O_3} \\ & + x\mathrm{BaTiO_3} + 2x\mathrm{BaO} + x/2\mathrm{O_2}. \end{aligned} \tag{9}$$

According to Eq. (9), we speculate that the Bi^{3+} ions enter into the A site of $BaTiO_3$ and the Bi^{5+} cations are incorporated into the B site, the segregated Ti^{4+} ions in the two formulas $(Ba^{2+}_{1-x}Bi^{3+}_x)[Ti^{4+}_{1-x}(Ti^{4+}\cdot \mathrm{e})_x]O_3$ and $Ba^{2+}[Ti^{4+}_{1-2x}Bi^{5+}_x(Ti^{4+}\cdot \mathrm{e})_x]O_3$ can play a key part in the formation of the bismuth layer-structured $Bi_4Ti_3O_{12}$ (BTO) with higher phase temperature ($T_c = 675$ °C. Hence, the $Bi_4Ti_3O_{12}/BaTiO_3$ (BTO–BT) composite material similar to BNT–BT ceramic will achieve higher phase transition temperature than the common semiconducted $BaTiO_3$ with $T_c = 120$ °C–130 °C. Of course, for a more reasonable understanding further investigation is needed.

4. Conclusions

In the present work, high T_c lead-free BB–BT ceramic is fabricated with a PTCR effect above 155 °C, using a conventional sintering technique in air atmosphere. For the first time a high T_c lead-free PTC ceramic with $T_c = 155$ °C can be directly sintered in air, which is obviously different from the BNT–BT system. The BB–BT ceramic exhibits a PTCR jump of approximately two orders of magnitude starting at 155 °C. The impedance analyses indicate that below T_c, the electrical response of the PTC ceramic is composed mainly of the three parallel RQ components in series (i.e. grain boundary, grain and grain shell); above T_c, the electrical response contributions are attributed mainly to the grain boundary and the grain. The fitting results by a complex nonlinear least squares fitting method are in good agreement with the experimental data. The grain boundary properties exhibit a positive temperature coefficient thermistor behaviour with $T_c = 155$ °C, which is the same as that of the bulk. With the increase of measured temperature, the extent to which the peaks of $\mathrm{Im}M(\omega)$ and $\mathrm{Im}Z(\omega)$ curves in Fig. 4 are matched indicates the occurrence from the localized to probable delocalized conduction mechanism.

In conclusion, the PTCR characteristics compared with those of the existing lead-contained PTCR ceramic and BNT–BT thermistor, indicate that the BB–BT system may be a promising lead-free material for implementable industrial utilization as a PTC thermistor with $T_c > 130$ °C.

References

[1] Urek S and Drofenik M 1999 *J. Euro. Ceram. Soc.* **19** 913

[2] Zajc I and Drofenik M 1998 *J. Mater. Res.* **13** 660

[3] Gillot C, Michenaud J P, Baukens I and Duvigneaud P H 1997 *J. Am. Ceram. Soc.* **80** 1043

[4] Qi J Q, Gui Z L, Wu Y J and Li L T 2002 *Mater. Chem. Phys.* **73** 97.

[5] Hill D and Tuller H 1991 *Ceramic Sensors: Theory and Practice* (New York: Marcel Dekker Inc.) p. 335

[6] Takeda H, Aoto W and Shiosaki T 2005 *Appl. Phys. Lett.* **87** 102104

[7] Shimada T, Touji K, Katsuyama Y, Takeda H and Shiosaki T 2007 *J. Euro. Ceram. Soc.* **27** 3877

[8] Xiang P H, Takeda H and Shiosaki T 2007 *Appl. Phys. Lett.* **91** 162904

[9] Xiang P H, Takeda H and Shiosaki T 2008 *J. Appl. Phys.* **103** 064102

[10] Xiang P H, Harinak H, Takeda H, Nishida T, Uchiyama K and Shiosaki T 2008 *J. Appl. Phys.* **104** 094108

[11] Yuan C L, Liu X Y, Ma J F and Zhou C R 2010 *Acta Phys. Sin.* **59** 4253 (in Chinese)

[12] Yuan C L, Liu X Y, Yang Y, Xu J W and Gu Y 2010 *Acta Phys. Sin.* **59** 7396 (in Chinese)

[13] Heywang W 1961 *Solid State Electron.* **3** 51

[14] Heywang W 1964 *J. Am. Ceram. Soc.* **47** 484

[15] Jonker G H 1964 *Solid State Electron.* **7** 895

[16] Kulwicki B M and Purdes A J 1970 *Ferroelectrics* **1** 253

[17] Ihrig H and Puschert W 1977 *J. Appl. Phys.* **48** 3081

[18] Cole K S and Cole R H 1941 *J. Chem. Phys.* **9** 341

[19] Sinclair D C and West A R 1989 *J. Appl. Phys.* **66** 3850

[20] Gerhardt R 1994 *J. Phys. Chem. Solids* **55** 1491

[21] Cao W and Gerhardt R 1990 *Solid State Ionics* **42** 213

[22] Lanfredi S and Nobre M A L 2005 *Appl. Phys. Lett.* **86** 081916

[23] Cox D E and Sleight A W 1979 *Acta Crystallogr.* B **34** 1

[24] Steigelmann O and Goertz P 2004 *Key Eng. Mater.* **264–268** 1161

[25] Luo Y, Liu X Y, Li X Q and Liu G Z 2006 *Solid State Ionics* **177** 1543